Infrared nitrogen-perturbed NO linewidths in a temperature range of atmospheric interest: An extension of the exact trajectory model

J. Buldyreva,* S. Benec'h, and M. Chrysos
Laboratoire des Propriétés Optiques des Matériaux et Applications, Unité Mixte de Recherche UMR CNRS 6136, Université d'Angers, 2 Boulevard Lavoisier, 49045 Angers, France
(Received 27 April 2000; published 11 December 2000)

Infrared NO-N_2 line-broadening coefficients for the fundamental 1-0 band are *ab initio* computed by means of the exact trajectory model extended to the case of a symmetric top active molecule. As intermolecular potential, the sum model composed of long-range dipole-quadrupole and quadrupole-quadrupole interactions as well as short-range atom-atom interactions, is taken. Line-broadening coefficients for both *R* and *P* branches of diamagnetic $^2\Pi_{1/2}$ and paramagnetic $^2\Pi_{3/2}$ sub-bands are reported for various temperatures in the range 163–296 K, thus significantly improving available theoretical results in the common temperature domain, while proposing values for temperatures that as yet have not been studied. The computed results are found to be in good agreement with a bulk of the experimental data.

DOI: 10.1103/PhysRevA.63.012708 PACS number(s): 34.10.+x, 33.70.Jg

I. INTRODUCTION

A variety of simple molecules exists which are particularly challenging for atmospherical purposes, whose rotational constants are small. The diatomics N_2, O_2, and NO as well as the triatomic CO_2 are representative members of this class. Due to their small rotational constants the number of relaxation channels in these systems increases rapidly even at not too high temperatures, making any rigorous quantum-mechanical tool, such as close-coupling and coupled states techniques practically inapplicable. In contrast, semiclassical methods offer themselves as the only valuable approach for the description of collisional line broadening (the Doppler effects are negligible for the pressure range to be considered here), provided the thermal energy coresponding to the temperature of the medium (kT) is sufficiently higher than the depth of the isotropic intermolecular potential well.

For many years the approach initially developed by Anderson [1] and later systematized by Tsao and Curnutte [2] was the only semiclassical theory available in the literature for an *ab initio* calculation of widths and shifts of isolated spectral lines; it is often referred to as the Anderson-Tsao-Curnutte (ATC) theory. As it is based on perturbation theory, only long-range intermolecular forces are taken into account and straight line molecule paths are employed. On practical grounds, it turns out that the ATC approach is suitable for systems interacting by strong electrostatic forces. In order to avoid divergencies of the scattering operator, which appear at small values of the impact parameter, an artificial ''cutoff'' procedure is imposed.

An important leap ahead in semiclassical studies was made a couple of decades ago by Robert and Bonamy [3]. In their work they showed that the unphysical cutoff procedure can be avoided by applying the linked cluster theorem of Kubo [4], resulting in a scattering operator of exponential form. In addition, they introduced a trajectory model of parabolic molecule paths. According to this model the curvature of the trajectory is produced by the influence of the isotropic potential, enabling one to include anisotropic short-range interactions for which atom-atom potential models can be employed. Compared to the ATC theory, the final expressions of the Robert-Bonamy (RB) formalism are rather complicated but analytical. The RB approach was then successfully applied to various molecular systems (diatom-diatom, diatom-noble gas, etc.) for which collisions at close approach are of great importance, especially for diagnostic purposes at high temperatures.

For the majority of the aforementioned molecular systems, however, the atmospheric temperatures correspond to kinetic energies (more or less) close to the isotropic potential well threshold. Therefore, as temperature decreases, the RB approach is expected to progressively lose its accuracy, becoming unable to provide meaningful predictions of linewidths. Given the fact that quantum mechanics is difficult to apply, a further refinement of the semiclassical description appears to be of particular interest.

As a next step, in 1992, Bykov *et al.* [5,6] proposed to apply directly the well-known exact solution of the equations of motion of a classical particle influenced by the isotropic potential [7], thus accessing an ''exact'' trajectory, yet valid within classical mechanics only. However, Bykov and coworkers performed no computation of linewidths. An attempt to introduce this exact trajectory model in the calculation of the second order contributions to the broadening cross section was undertaken by one of us in collaboration with Bonamy and Robert in the framework of the RB formalism [8]. In that work the isotropic linewidths of self-perturbed nitrogen were calculated at low and room temperatures as a function of the rotational quantum number. The results obtained from these computations were much more realistic than those from any previous approach based on other trajectory models, and clearly demonstrated the advantage of the new approach. Since the exact trajectory model is reli-

*Corresponding author. Email address: jeanna.buldyreva@univ-angers.fr

able, the conclusion was drawn that an appropriate application of the exact trajectory model can be made provided the representation of the atom-atom interactions in the intermolecular potential is equally accurate.

The aim of the present paper is twofold. On the one hand, from a purely fundamental viewpoint, an extension of the exact trajectory approach is made to a more general (and complicated) case of symmetric top active molecules which are frequently involved in atmospheric processes. It should be mentioned that such a symmetric top extension has already been realized in the framework of the RB formalism but for a parabolic trajectory [9]. A couple of years later, an application was made to the infrared (IR) NO-N_2 and NO-O_2 linewidth coefficients [10]; but only a few theoretical values were reported therein and, for the two temperatures studied (295 and 163 K), the predicted linewidths for high rotational levels were too small in comparison with experiment. On the other hand, from the practical point of view, the fact that theoretical estimations of NO-N_2 (-O_2, -air) linewidths included in the HITRAN-96 database [11] are either too rough or even unavailable, makes an appropriate *ab initio* calculation particularly challenging. We note that this case of NO perturbed by the linear molecules N_2 and O_2 is of great importance due to the dominant concentrations of nitrogen and oxygen in the Earth's atmosphere (about 79% and 21% respectively); the concentration of the active molecule NO is very low and the role of NO-NO collisions is negligible.

This paper is organized as follows. In Sec. II, the basic points of the exact trajectory implementation in the RB approach adapted to the case of NO are briefly discussed. In Sec. III the linewidths for both *R* and *P* branches of the 1-0 diamagnetic $^2\Pi_{1/2}$ and paramagnetic $^2\Pi_{3/2}$ sub-bands are calculated, analyzed in detail, and compared with a bulk of experimental data available for different temperatures [10,12,13]. Concluding remarks and further perspectives of exact-trajectory modeling are collected in the last section.

II. GENERAL FORMALISM

A. Semiclassical approach of Robert and Bonamy for a symmetric top active molecule

The semiclassical formalism of Robert and Bonamy [3] was initially developed for linear molecules in the fundamental Σ state. For this purpose, the so-called *classical path* assumption was made, i.e., the angular momenta tied to the active molecule and to the perturber were decoupled. This is equivalent to saying that the internal angular momenta for each molecule are much smaller than the total angular momentum, and that the orbital momentum is sufficient to provide a realistic description of the rotational part of the relative motion.

In the framework of this approach, for any-type spectrum, the linewidth γ_{fi} (in cm^{-1}) associated with optical transition $(i \to f)$ is given by

$$\gamma_{fi}=\frac{n_b}{2\pi c}\sum_{v_2,j_2}\rho_{v_2 j_2}\int_0^\infty v f(v)dv\int_0^\infty 2\pi b db \times\{1-[1-S^{(L)}_{2,f2i2}]\exp[-(S_{2,f2}+S_{2,i2}+S^{(C)}_{2,f2i2})] \times\cos[(S_{1,f2}+S'_{2,f2})-(S_{1,i2}+S'_{2,i2})]\}. \quad (1)$$

Here, n_b is the numerical density of the perturbing particles and $\rho_{v_2 j_2}$ is their thermal population. In practice, the integration over relative velocity v with the Maxwell-Boltzmann distribution $f(v)$ is replaced by the mean thermal velocity $\overline{v}=\sqrt{8kT/\pi m^*}$ (T is the temperature and m^* is the reduced mass of the molecular pair). The integral over impact parameter b is replaced by the integral over the distance of the closest approach r_c (see, for more details, Ref. [3]), where r_c and b are related with each other via the energy conservation condition

$$b/r_c=\sqrt{1-V^*_{\mathrm{iso}}(r_c)}.$$

An asterisk denotes the potential's reduced value defined by $V^*_{\mathrm{iso}}=2V_{\mathrm{iso}}/m^*v^2$.

The isotropic part of the intermolecular potential V_{iso} appearing in the above expression is usually represented by a Lennard-Jones dependence $V_{\mathrm{LJ}}(r)=4\varepsilon[(\sigma/r)^{12}-(\sigma/r)^6]$ where ε and σ are two parameters designating the depth of the potential well and the radius of the action of the repulsive forces, respectively. Since V_{iso} does not depend on the vibrational coordinates of the active molecule, the first-order purely vibrational contribution $S_{1,f2}-S_{1,i2}$ in Eq. (1) vanishes. For linewidths, the imaginary part of the second-order contribution $S'_{2,f2}-S'_{2,i2}$, which results from the noncommutative character of the interaction potential and which is essential for lineshift calculations, can be neglected. Finally, the assumption is made that only rotational transitions are induced by collisions in the perturbing molecule and that no summation on the vibrational quantum number v_2 is needed. With all the abovementioned remarks, for the IR absorption case Eq. (1) is transformed into

$$\gamma_{fi}=\frac{n_b v}{2\pi c}\sum_{j_2}\rho_{j_2}\int_{r_{c,\min}}^\infty 2\pi r_c dr_c\left\{1+\frac{8\varepsilon}{m^*v^2}\times\left[5\left(\frac{\sigma}{r_c}\right)^{12}-2\left(\frac{\sigma}{r_c}\right)^6\right]\right\} \times\{1-[1-S^{(L)}_{2,f2i2}]\exp[-(S_{2,f2}+S_{2,i2}+S^{(C)}_{2,f2i2})]\}, \quad (2)$$

where the low bound $r_{c,\min}=\sigma[2/(1+\sqrt{1+m^*v^2/2\varepsilon}]^{1/6}$.

The first two contributions appearing in the exponential of Eq. (2) are analogous to the ''outer'' terms $S^{\mathrm{outer}}_{2,f}, S^{\mathrm{outer}}_{2,i}$ of the ATC theory, while the last one $S^{(C)}_2$ corresponds to that part of the Anderson ''middle'' term S^{middle}_2 which is diagonal in the quantum numbers of the perturbing molecule; $S^{(L)}_2=S^{\mathrm{middle}}_2-S^{(C)}_2$ [14]. All these contributions are given explicitely by the following relationships [3]:

$$S_{2,i2}=\frac{\hbar^{-2}}{2(2j_i+1)(2j_2+1)}\sum_{\substack{j_i'j_2'\\ m_im_i'm_2m_2'}}\left|\int_{-\infty}^{+\infty}dt\,\exp(i\omega_{j_ij_2,j_i'j_2'}t)\langle j_im_ij_2m_2|V_{\text{aniso}}(r(t))|j_i'm_i'j_2'm_2'\rangle\right|^2, \tag{3}$$

$$S^{(C)}_{2,f2i2}=\sum_{j_2'}S_{2,f2'i2'}\delta_{j_2'j_2}, \tag{4}$$

$$S^{(L)}_{2,f2i2}=\sum_{j_2'\neq j_2}S_{2,f2'i2'}, \tag{5}$$

$$S_{2,f2'i2'}=-\frac{\hbar^{-2}}{(2j_i+1)(2j_2+1)}\sum_{\substack{m_im_i'm_fm_f'\\ m_2m_2'}}C^{j_im_i}_{j_fm_f\nu\rho}C^{j_im_i'}_{j_fm_f'\nu\rho}\int_{-\infty}^{\infty}dt\,\exp(i\omega_{j_2'j_2}t)\langle j_fm_f'j_2'm_2'|V_{\text{aniso}}(r(t))|j_fm_fj_2m_2\rangle$$
$$\times\int_{-\infty}^{\infty}dt'\,\exp(i\omega_{j_2j_2'}t')\langle j_im_ij_2m_2|V_{\text{aniso}}(r(t'))|j_im_i'j_2'm_2'\rangle. \tag{6}$$

In Eqs. (3),(6) j_i, j_f, j_2 and m_i, m_f, m_2 are the rotational and magnetic quantum numbers, respectively; ν is the order of the coupling tensor between the molecules and the external field; for the IR absorption case $\nu=1$. Primes mark values after collision. The $S_{2,f2}$ contribution for the final state f is given by simply changing i into f in Eq. (3). When switching (formally) to the case of a symmetric top active molecule, the corresponding rotational wave functions in Eqs. (3),(6) are no longer the same.

In the nitric oxide molecule, because of the strong coupling of the electronic orbital angular momentum along the intermolecular axis ($\Lambda=1$) with the corresponding spin angular momentum component $\Sigma=\pm 1/2$, the total electronic angular momentum component K can take values 1/2 or 3/2. So, the fundamental state is $^2\Pi$, with $^2\Pi_{1/2}$ levels lying lower than the $^2\Pi_{3/2}$ ones (normal structure). In addition, the interaction between the electronic orbital momentum and the rotational one results into a supplementary Λ doubling (λ-e and λ-f components) of each (J,K) level. The latter effect is rather small and has been observed in a few experiments only [12]. Since in the RB formalism this kind of coupling is neglected, λ-e and λ-f components are indistinguishable from the theoretical standpoint. The Λ-Σ coupling in NO is intermediate between the Hund cases (a) and (b), so the true wave functions should be linear combinations of symmetric top wave functions corresponding to the pure Hund case (a) for sublevels $K=1/2$ and $K=3/2$. Nevertheless, for not too high rotational quantum numbers J the mixing effects are minor and the pure Hund case (a) serves as a good approximation [15]. The wave functions $|JKM\rangle$ are thus supplied with three quantum numbers J, K, and M. We remind the reader that J is the total angular momentum, K is the projection of J along the molecular axis, and M is the projection of J along the laboratory z axis. To proceed further with the second-order contributions of Eqs. (3),(6), the intermolecular potential must be specified.

B. Intermolecular potential

A realistic description of the intermolecular potential plays a crucial role when a refined trajectory model is employed [8]. Unfortunately, no accurate *ab initio* potential for the NO-N_2 system has thus far been available, to our knowledge. In order to make a meaningful comparison of the results obtained with different trajectory models, keeping at the same time the advantages of an analytical potential expression, we retain the same representation of the intermolecular potential as in the work of Houdeau *et al.* [10]:

$$V_{\text{aniso}}(r)=V_{\text{el}}(r)+V_{\text{at-at}}(r)$$
$$=V_{\mu_1Q_2}+V_{Q_1Q_2}+\sum_{i,j}\left(\frac{d_{ij}}{r^{12}_{1i,2j}}-\frac{e_{ij}}{r^{6}_{1i,2j}}\right).$$

In the equation above, the long-range electrostatic part V_{el} is approximated by dipole-quadrupole ($V_{\mu_1Q_2}$) and

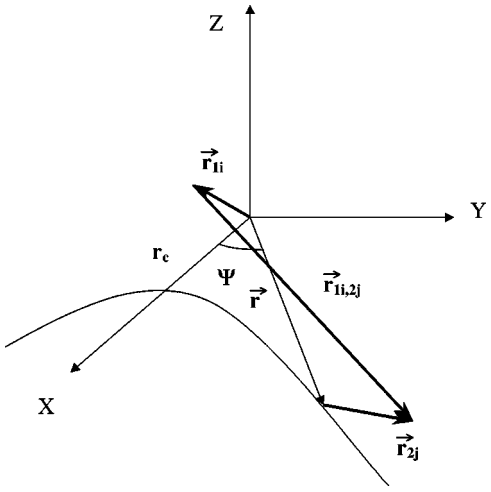

FIG. 1. Geometry of molecular collision in the laboratory fixed frame.

TABLE I. Physical parameters for NO-N_2 interaction potential; I and II stand for different parametrizations of $V_{\rm iso}$.

ε	σ	d_{ij}	e_{ij}	$\lvert r_{1i}\rvert$ (or $\lvert r_{2j}\rvert$)	Q	μ	B_0
K	Å	10^{-7} erg Å^{12}	10^{-10} erg Å^{6}	Å	10^{-26} esu	10^{-18} esu	cm^{-1}
118.8 (I)	3.58 (I)	$d_{\rm NN}=0.2910$	$e_{\rm NN}=0.2502$	$\lvert r_{1N}\rvert=0.614$	$Q_{\rm NO}=-1.8$	$\mu_{\rm NO}=0.158$	$B_{0\ \rm NO}=1.6957$
104.4 (II)	3.58 (II)	$d_{\rm NO}=0.1425$	$e_{\rm NO}=0.1911$	$\lvert r_{2N}\rvert=0.548$	$Q_{N_2}=-1.52$		$B_{0\ N_2}=2.01$
				$\lvert r_{2O}\rvert=0.603$			

quadrupole-quadrupole ($V_{Q_1Q_2}$) interactions; μ_k and Q_k stand for the dipole and quadrupole moments of the kth molecule, respectively. The short-range part $V_{\text{at-at}}$ is given by the sum of a pair of atomic Lennard-Jones dependences with the atomic pair energy parameters d_{ij} and e_{ij}; $r_{1i,2j}$ is the distance between the ith atom of the first molecule and the jth atom of the second one (see Fig. 1). $V_{\text{at-at}}$ is obviously composed of its repulsive V_D and attractive V_E parts: $V_{\text{at-at}} \equiv V_D + V_E$. All required parameters for the NO-N_2 potential are listed in Table I. There, the interatomic parameters d_{ij} and e_{ij} are low-limit values deduced from homonuclear diatomics data of Ref. [16] using the usual combination rules

$$r_{\omega,\rm NO}=(r_{\omega,\rm NN}+r_{\omega,\rm OO})/2,$$

$$e_{\rm NO}=(e_{\rm NN}e_{\rm OO})^{1/2},$$

$$d_{\rm NO}=e_{\rm NO}(2r_{\omega,\rm NO})^6/2$$

with $r_{\omega,X}$ being the van der Waals radius for the quasimolecule $X\ldots X$. It should be noted that the atom-atom parametrization for the NO case is rather complicated since no set of parameters was found to be compatible with the three sets of experimental data for N_2, O_2, and NO simultaneously [16]; for our calculations, the low-limit values were chosen since they are of the same order as those used commonly.

For further purposes, the dependence of each anisotropic potential term on the intermolecular vector modulus r and on the polar angle Ψ (see Fig. 1) should be written explicitly. To do this, we start from the most general form of the long-range interaction energy between two molecules (1 and 2) of an arbitrary symmetry [17] :

$$V(r)=\sum_{\substack{l_1l_2l\\ m_1m_2\mu_1\mu_2}} D^{l_1}_{-\mu_1,-m_1}(1)D^{l_2}_{-\mu_2,-m_2}(2)C^{lm}_{l_1m_1l_2m_2} \times C^{*}_{lm}(\Omega)\sum_n B^{(n)}_{l_1l_2l}(r)A^{(n)}_{l_1\mu_1}A^{(n)}_{l_2\mu_2}. \tag{7}$$

The orientation of molecules enters this expression through the Wigner rotational matrices $D^{l}_{m'm}(\psi,\vartheta,\phi)$, whose arguments are reversed for practical purposes[1]; (ϕ,ϑ,ψ) are the three Euler angles of the corresponding molecule relative to the laboratory axis. The intermolecular vector $\vec{r}=(r,\Omega)$ is characterized by the spherical harmonic $C_{lm}(\Omega)=\sqrt{4\pi/(2l+1)}Y_{lm}(\theta,\Psi)$; an asterisk accounts for complex conjugation. The coefficients $B^{(n)}(r)$ are defined by the interaction type n, $A^{(n)}$ are molecular parameters, and $C^{lm}_{l_1m_1l_2m_2}$ denote the Clebsh-Gordan coefficients [18].

The atom-atom potential dependence on r and Ψ can be obtained [8] by means of a two-center expansion [19]. Since in this case $r_{1i,2j}$ is defined by three vectors $\vec{r}_{1i}$, $\vec{r}_{2j}$, and $\vec{r}$, its nth inversed power appears as an infinite series of three spherical harmonics tied to these vectors orientations in the laboratory fixed frame:

$$\frac{1}{r^n_{1i,2j}}=\frac{1}{r^n}\sum_{l_1l_2l}(-1)^{l_2}C^{l0}_{l_10l_20}\sum_{p,q}\left(\frac{r_{1i}}{r}\right)^p\left(\frac{r_{2j}}{r}\right)^q\frac{(2l_1+1)(2l_2+1)(n+p+q-l-3)!!(n+p+q+l-2)!!}{(n-2)!(p-l_1)!!(p+l_1+1)!!(q-l_2)!!(q+l_2+1)!!}$$

$$\times\{1+\delta_{n,1}(\delta_{p,l_1}\delta_{q,l_2}\delta_{p+q,l}-1)\}\sum_{m_1m_2m}C^{lm}_{l_1m_1l_2m_2}C_{l_1m_1}(1)C_{l_2m_2}(2)C^{*}_{lm}(\Omega),$$

$$p=l_1,l_1+2,l_1+4,\ldots,$$

$$q=l_2,l_2+2,l_2+4,\ldots. \tag{8}$$

For practical calculations this series has to be truncated. For our purposes we limit ourselves to the leading ($p=l_1,q=l_2$) and first correction ($p=l_1,q=l_2+2$; $p=l_1+2,q=l_2$) repulsive ($V_D^{(0)},V_D^{(1)}$) and attractive ($V_E^{(0)},V_E^{(1)}$) terms only. For $l_1=l_2=2,l=4$, their explicit expressions can be found in Ref. [8]. Contributions of higher order are estimated to be negligible. We note that the single difference between the structure of the atom-atom interaction energy expression and that of the long-range energy of Eq. (7) is that the mo-

[1]These two forms are related by $D^{l}_{m,m}(\psi,\vartheta,\phi)=(-1)^{m'-m}D^{l}_{mm'}(\phi,\vartheta,\psi)$[17].

lecular moments (or polarizabilities) As are replaced by combinations of atomic parameters $d_{ij}, e_{ij}, r_{1i}, \ldots$ etc.

The representation of the interaction potential as a series of products of rotational matrices (or of spherical harmonics) leads immediately to the conclusion that, according to orthogonality properties, only contributions of the same tensorial rank $(l_1 l_2 l)$ are able to generate cross terms. For example, the electrostatic quadrupole-quadrupole term and the atom-atom one of the same symmetry (224) interfere to give a cross-term proportional to the product of matrix elements of V_{el}^{224} and $V_{\text{at-at}}^{224}$.

C. Calculation of matrix elements

For a symmetric top active molecule the angular dependence of rotational wave functions is given by

$$|JKM\rangle = \left(\frac{2J+1}{8\pi^2}\right)^{1/2} D^J_{-K,-M}(\psi,\vartheta,\phi).$$

In the case of the long-range potential of Eq. (7), the corresponding matrix elements of Eqs. (3),(6) can thus be expressed [17] via the Wigner-Eckart theorem

$$\langle J'K'M'|D^l_{-k,-m}|JKM\rangle = \frac{(J'K':|D^l_{-k\cdot}|:JK)}{\sqrt{2J'+1}} C^{J'M'}_{JMlm},$$

where the double dots in the numerator serve to distinguish the reduced matrix element in M space. Using the definition

$$\sum_{\mu_1} A^{(n)}_{l_1\mu_1}(J'K':|D^l_{-k\cdot}|:JK) \equiv A^{(n)}_{l_1}(J'K';JK)$$

and taking into account that for $l_1 \leqslant 2$ there is at most one nonvanishing molecular parameter, one obtains [17]

$$A^{(n)}_{l_1}(J'K';JK) = A_{l_1 0}\sqrt{2J+1}\, C^{J'K'}_{JKl_1 0}\delta_{KK'},$$

where for electrostatic interactions $A^{(\mathrm{electr})}_{10} = \mu$, $A^{(\mathrm{electr})}_{20} = Q$, $A^{(\mathrm{electr})}_{30} = \Xi$, etc., that is, respectively, dipole, quadrupole, octupole moments. From the equation above, it can also be seen that for the symmetric top active molecule only transitions inside each sub-band are allowed: $K' = K$.

Then, for example, in the case of NO-N_2, the outer term for electrostatic $(l = l_1 + l_2)$ interactions $S_{2,i2}$ can be written as

$$S^{\mathrm{el}}_{2,i} = \hbar^{-2} \sum_{l_1 l_2 l} (A^{(n)}_{l_1 0})^2 (A^{(n)}_{l_2 0})^2 \sum_{j_i' j_2'} (C^{j_i' K}_{j_i K l_1 0})^2 (C^{j_2' 0}_{j_2 0 l_2 0})^2 \tilde{f}^{\mathrm{el}}_{l_1 l_2 l}, \tag{9}$$

where the corresponding electrostatic resonance function $\tilde{f}^{\mathrm{el}}_{l_1 l_2 l}$ is introduced as follows:

$$\tilde{f}^{\mathrm{el}}_{l_1 l_2 l} \equiv \frac{(2l)!}{2(2l_1+1)!(2l_2+1)!} \sum_m \int_{-\infty}^{+\infty} dt \times \exp[i(\omega_{ii'} + \omega_{22'})t] \frac{C^*_{lm}(\Omega)}{r^{l+1}} \int_{-\infty}^{+\infty} dt \times \exp[-i(\omega_{ii'} + \omega_{22'})t] \frac{C_{lm}(\Omega)}{r^{l+1}}, \tag{10}$$

Comparing Eq. (9) with its analog from Ref. [8], it is ascertained, as expected, that the difference with the case of a linear active molecule is contained in the Clebsch-Gordan coefficients for the active molecule, which now depend on the quantum number K.

For the atom-atom contributions the corresponding matrix element reads [2]

$$\langle J'K'M'|Y_{lm}|JKM\rangle = \sqrt{\frac{2l+1}{4\pi}}\sqrt{\frac{2J+1}{2J'+1}} C^{J'K'}_{JKl0} C^{J'M'}_{JMlm},$$

which results in a K dependence of appropriate second-order contributions totally analogous to the long-range interaction case. The K dependence of connected and linked terms is defined by the D factor (see Ref. [3])

$$D^{(l_1)} = (-1)^{j_i + j_f} 2[(2j_i+1)(2j_f+1) \times (C^{j_i K}_{j_i K l_1 0})^2 (C^{j_f K}_{j_f K l_1 0})^2]^{1/2} W(j_i j_f j_i j_f; \nu l_1),$$

where W is the Racah coefficient (K independent) and ν is the order of the coupling tensor between the molecule and the external field.

D. Exact trajectory modeling

To carry out the time integration in the resonance functions [see, for example, Eq. (10)] the trajectory model should be chosen. For a straight-line trajectory or a parabolic shape one the integration is quite simple leading to analytical expressions, whereas for the exact trajectory the procedure is rather complicated and should be performed numerically. The exact solution of classical equations of motion governed by an isotropic potential gives the time t and the phase Ψ as functions of the intermolecular distance r [7]:

$$t(r) = \int_{r_c}^{r} \frac{dr'}{\sqrt{2[E - V_{\mathrm{iso}}(r')]/m^* - M^2/m^{*2} r'^2}} + c_1, \tag{11}$$

$$\Psi(r) = \int_{r_c}^{r} \frac{M/m^* r'^2 dr'}{\sqrt{2[E - V_{\mathrm{iso}}(r')]/m^* - M^2/m^{*2} r'^2}} + c_2. \tag{12}$$

Here $E = m^* v^2/2$ and $M = m^* b v$ are the energy and angular momentum of the colliding pair, respectively. Let us now consider that the collision takes place in the plane XOY (Fig. 1), so that at $t = 0$ we have $r = r_c$ and $\Psi = 0$. Hence, in Eqs. (11),(12), the integration constants c_1 and c_2 vanish. In order

to address a larger audience, it is noteworthy that, by means of Eq. (11), the integration over t in Eq. (10) can be replaced by the integration over r through

$$dt = dr/\sqrt{2[E - V_{\rm iso}(r)]/m^* - M^2/m^{*2}r^2}.$$

In addition, for the specific axes orientation of Fig. 1 ($\theta = \pi/2$) the angular dependence of spherical harmonic C_{lm}

$$C_{lm}(\theta,\Psi) = \left[\frac{(l-m)!}{(l+m)!}\right]^{1/2} e^{im\Psi} P_l^m(\cos\theta)$$

can be simplified since only the pair sums of l and m give nonzero contributions in the associated Legendre polynomials

$$P_l^m(0) = \frac{(-1)^{(l+m)/2}}{2^l} \frac{(l+m)!}{[(l-m)/2]![(l+m)/2]!}.$$

Additionally, as the trajectory is symmetric relatively to $\vec{r}_c$, each of the integrals over time in Eq. (9) can be replaced by its integral equivalent from zero to infinity. Their product can be further written as the squared value of the integral of $\cos[\omega t + m\Psi(r(t))]/r^{l+1}$, whose arguments are given in the exact trajectory approach by

$$\omega t = k_c \int_1^y \frac{z\,dz}{\{z^2 - 1 + V_{\rm iso}^*(r_c) - z^2 V_{\rm iso}^*(z r_c)\}^{1/2}}, \quad k_c = \omega r_c / v,$$

$$m\Psi = m \int_1^y \frac{\{1 - V_{\rm iso}^*(r_c)\}^{1/2} dz}{z\{z^2 - 1 + V_{\rm iso}^*(r_c) - z^2 V_{\rm iso}^*(z r_c)\}^{1/2}}.$$

Then, the final exact trajectory expression for the electrostatic resonance function reads

$$\tilde{f}^{\rm el}_{l_1 l_2 l} \equiv \frac{1}{v^2 r_c^{2l}} f^{\rm el}_{l_1 l_2 l},$$

$$f^{\rm el}_{l_1 l_2 l}(k_c, r_c, v) = \frac{2(2l)!}{(2l_1+1)!(2l_2+1)!} \sum_{\substack{m \\ l+m \text{ even}}} \frac{(l+m)!(l-m)!}{2^{2l}[(l-m)/2]!^2[(l+m)/2]!^2} \times \left[\int_1^\infty dy \frac{\cos[A_0(y)k_c + m\{1 - V_{\rm iso}^*(r_c)\}^{1/2} A_2(y)]}{y^l\{y^2 - 1 + V_{\rm iso}^*(r_c) - y^2 V_{\rm iso}^*(y r_c)\}^{1/2}}\right]^2,$$

$$A_n(y) = \int_1^y \frac{dz}{z^{n-1}\{z^2 - 1 + V_{\rm iso}^*(r_c) - z^2 V_{\rm iso}^*(z r_c)\}^{1/2}}, \tag{13}$$

where $y \equiv r/r_c$. Variable $k_c = (\omega_{ii'} + \omega_{22'}) r_c / v$ plays the role of the dynamic resonance parameter and characterizes how close the pairs of states ii' and $22'$ are to the exact resonance. All the resonance functions as well as the corresponding second-order contributions taken into account in the present calculation, are collected in the Appendix.

III. APPLICATION TO THE NO-N_2 CASE

To check the extended exact-trajectory model developed above, we calculate by means of Eq. (2) the IR line broadening coefficients for the NO-N_2 system in a temperature ranging from 163 to 296 K, for which various experimental data are available [10,12,13]. The results are plotted on Figs. 2–6 and some representative numerical values are listed in Tables II–V.

The room temperature case is studied first, for which three sets of experimental data have been obtained by Houdeau *et al.* [10] (295 K), Spencer *et al.* [12] (296 K), and Ballard *et al.* [13] (296 K). In Ref. [10] only a few R-branch linewidths of $^2\Pi_{1/2}$ and $^2\Pi_{3/2}$ sub-bands have been measured, and some $^2\Pi_{3/2}$ sub-band linewidths have been calculated by the RB approach with a parabolic trajectory (PT) model; more complete theoretical PT results can be found in Ref. [9]. These data are plotted in Figs. 2(a) and 2(b) (for $K = 1/2$ and $K = 3/2$ cases, respectively) together with our exact trajectory (ET) results; the corresponding numerical values are listed in Tables II and III. In order to make a meaningful comparison between the results obtained by the two trajectory models, i.e., the PT and the ET ones, we use for this temperature the same parametrization of $V_{\rm iso}$ as in Refs. [9] (denoted by I in Table I). To analyze how linewidth coefficients are influenced by short range interactions, we proceed in our calculation by progressively taking into account the different force-field contributions pertaining to the collision. We start by pure electrostatic (224) and (123) terms, then add the corresponding atom-atom and cross terms, and end up with the (121) atom-atom ones. The latter contribution, with no electrostatic analog, is shown here to be almost negligible even for high rotational quantum numbers; this fact justifies that the atom-atom series of Eq. (8) has practically converged. In what follows, the three abovementioned sets of contributions are denoted by ET″, ET′, and ET, respectively. As one can see from Fig. 2, for low rotational quantum numbers the ET″ term dominates, whereas for high J it is unable to reproduce alone; the observed linewidths; this feature has been observed already within the PT model

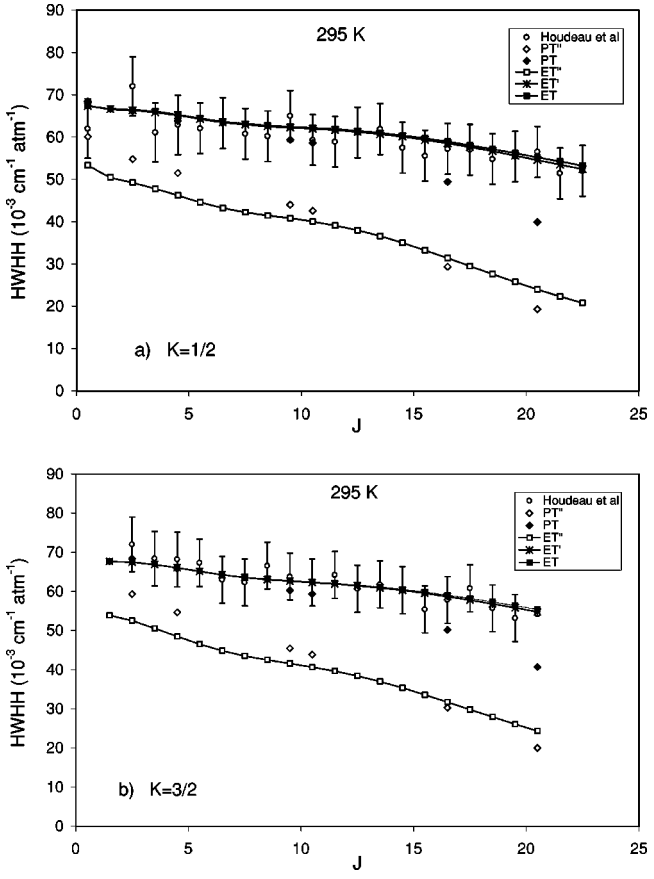

FIG. 2. Line-broadening coefficients as a function of the rotational quantum number for the fundamental band of NO perturbed by N_2 (R branch) at 295 K: (a) $^2\Pi_{1/2}$ sub-band, (b) $^2\Pi_{3/2}$ sub-band.

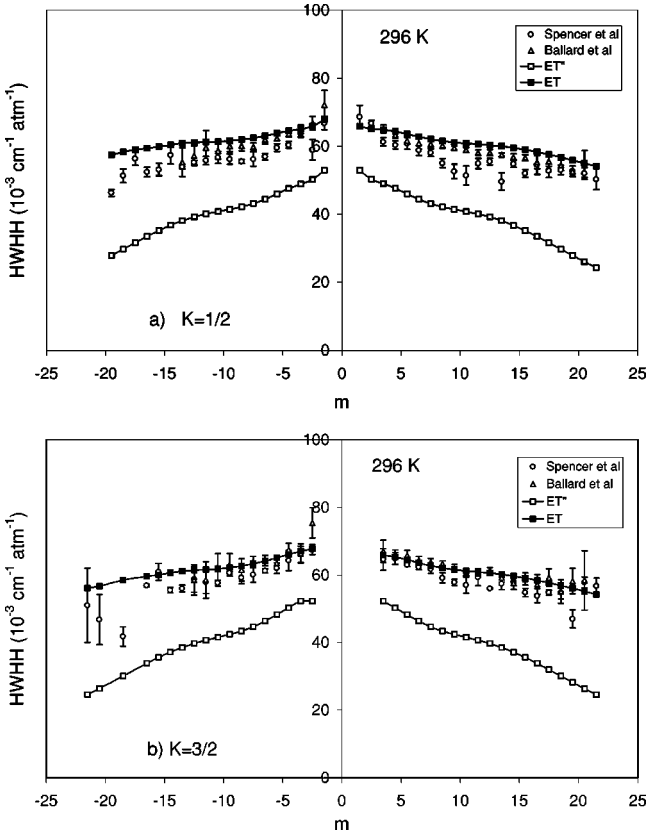

FIG. 3. Line-broadening coefficients as a function of m ($m=-J$ for $\Delta J=-1$ and $m=J+1$ for $\Delta J=+1$) for the fundamental band of NO perturbed by N_2 at 296 K: (a) $^2\Pi_{1/2}$ sub-band, (b) $^2\Pi_{3/2}$ sub-band.

[9,10] (PT″-points on the figures). Indeed, as far as the high J values are concerned, rotational energy spacings are large, thus requiring a violent (energetic) collision to occur in order for the nonoptical transitions to be realized. Since these violent collisions probe intermolecular distances of close approach, for which atom-atom interactions are mainly responsible, the role of the corresponding contributions for high rotational numbers becomes crucial and can no longer be neglected. When the atom-atom and cross terms (224) and (123) are included (ET′), excellent agreement with experiment is found, in contrast to the PT model which obviously fails for high J. Addition of (121) atom-atom contributions does not influence greatly this result (see ET curves in Fig. 2). It is also noteworthy that the computed line-broadening coefficients get slightly larger values for $K=3/2$ as compared to the $K=1/2$ case (see Tables II,III). This exaltation of linewidth, when passing from the $^2\Pi_{1/2}$ sub-band to the $^2\Pi_{3/2}$ one (for a given rotational transition), is well known. It was observed experimentally many years ago [20,21] and equally reproduced by the PT model calculation [10].

As was mentioned above, at 296 K, exhaustive experimental studies have been realized for both R and P branches [12,13] allowing us to carry out a more thorough theoretical analysis. The ET values computed in the present work for this temperature are listed in Tables IV and V, and plotted in Figs. 3(a) and 3(b), together with experimental data, against the quantum number m. We remind the reader that for the P branch, $m=-J$, while in the R branch it is $m=J+1$. Since no PT calculations have been realized at this temperature, the parametrization II (see Table I) for ε and σ, deduced by combination rules from Ref. [24], was made as it was more appropriate for the temperature range studied. In comparison with the measurements of Spencer *et al.* [12], for the $K=1/2$ case [Fig. 3(a)] our theoretical values seem to be overestimated for intermediate values of $|m|$. Nevertheless, they are very close to the experimental results of Ballard *et al.* [13]. For the $K=3/2$ sub-band [Fig. 3(b)] the ET predictions demonstrate a very good agreement with both experimental sets.

For all other temperatures studied (see Figs. 4–6), given that fewer (or even no) straightforward experimental mesurements have been realized, we widened the set of available experimental data by scaling the results of Ballard *et al.* from 296 K to the temperatures of interest by the well-known empirical relation

$$\gamma_J(T)=\gamma_J(T_0)\left(\frac{T}{T_0}\right)^{n(J)}$$

with the temperature exponents $n(J)$ taken from Ref. [13]. We note that at 183 K [Figs. 5(a),5(b)] Spencer *et al.* [12] succeeded in experimentally resolving both e-λ and f-λ

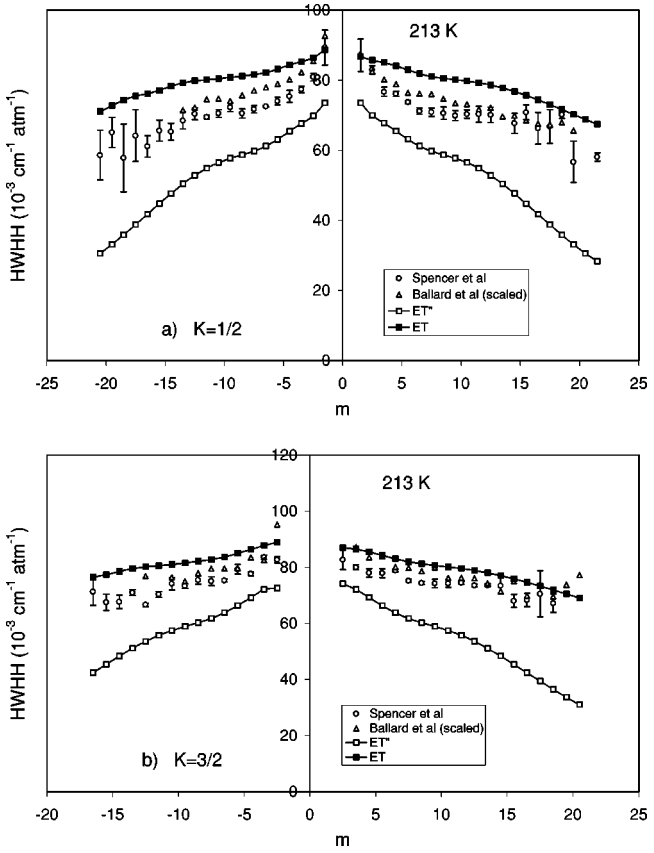

FIG. 4. Line-broadening coefficients as a function of m for the fundamental band of NO perturbed by N_2 at 213 K: (a) $^2\Pi_{1/2}$ sub-band, (b) $^2\Pi_{3/2}$ sub-band.

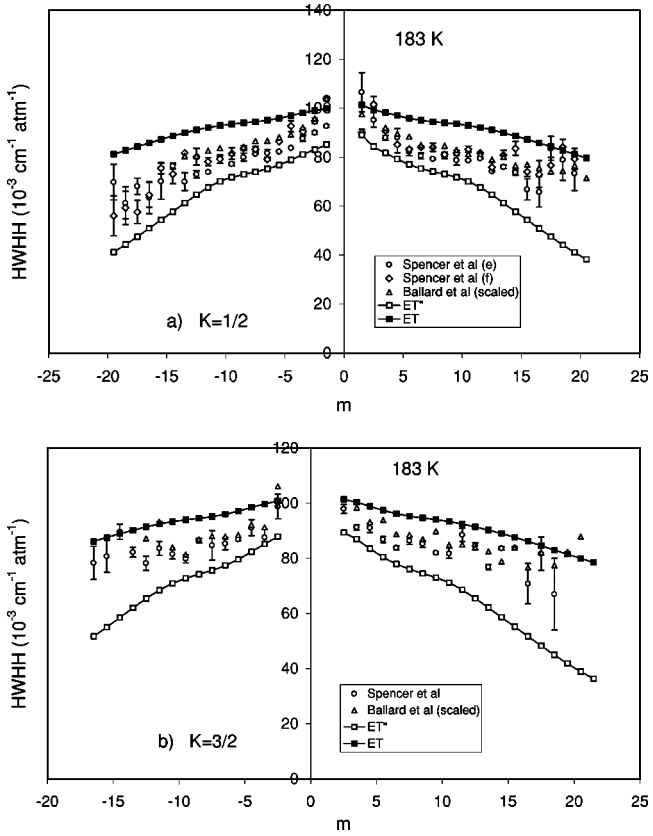

FIG. 5. Line-broadening coefficients as a function of m for the fundamental band of NO perturbed by N_2 at 183 K: (a) $^2\Pi_{1/2}$ sub-band, (b) $^2\Pi_{3/2}$ sub-band; (e) and (f) sets of the experimental data of Spencer *et al.* mark the λ-e and λ-f components.

components of $^2\Pi_{1/2}$ transitions, but these Λ doubling effects are not incorporated in the semiclassical formalism used here and cannot be distinguished from a theoretical standpoint. It can be stated from Figs. 4–6, that with decreasing temperature the ET model tends to overestimate the line-broadening coefficients for intermediate $|m|$ in the $K=1/2$ cases, but yields nearly realistic predictions for $K=3/2$; the slope of theoretical curves is quite correct in all cases studied. We ascribe this overestimation to be due to the roughness and imperfection of the initial potential model but not to the failure of the ET approach. As can be seen from Fig. 6(b) (163 K), where the PT results [10] are plotted for comparison, even at low temperatures the present trajectory modeling remains much more useful.

The adequacy of the ET modeling itself is additionally confirmed by the fact that our calculation reproduces completely the ''shoulder'' in the γ dependence on $|m|$, which has been clearly observed experimentally. This shoulder feature has been interpreted by Bouanich and Blanquet [22] as being due to the predominant influence of resonant (energy transfer) quadrupole-quadrupole interactions. A theoretical expression to evaluate the $J_{\max}$ value for which the resonant interaction is maximum can also be found in Ref. [23]:

$$J_{\max}^{l_1 l_2} = \frac{B_2 l_2}{B_1 l_1} J_{2\max},$$

where B_1 and B_2 are, respectively, the rotational constants for the active and perturbing molecules, l_1 and l_2 stand for the orders of corresponding spherical harmonics, and $J_{2\ \max}$ is the most populated state of the pertuber at a given temperature. For the quadrupole-quadrupole interactions ($l_1 = l_2 = 2$) the $J_{\max}^{22}$ values calculated by the above equation are 7.5 (296 K), 6.5 (213 K), 6.5 (183 K), and 5.5 (163 K). These values correspond exactly to the starting point of the shoulders obtained with our ET modeling. For the dipole-quadrupole interaction case, the previous $J_{\max}^{22}$ values should simply be doubled ($l_1=1, l_2=2$) and one obtains $J_{\max}^{12}$ marking the end of shoulders. Nevertheless, the dipole-quadrupole interactions seem to us to be too weak to condition the resonant energy transfer in the NO-N_2 case, and more complicated mechanisms involving short-range forces should be responsible for the formation of shoulders at such high rotational numbers.

The last point to enlighten concerns the general observation that the ET model reproduces better the $K=3/2$ case than the $K=1/2$ one. This feature, which in the framework of previous semiclassical approaches has to our knowledge never been observed, looks at first sight quite surprising. Indeed, from the standpoint of a linear molecule ($K=0$) one should expect better results for the lowest fundamental sub-band ($K=1/2$). However, a deeper analysis of the basic classical approximations (see the first paragraph of Sec. II) re-

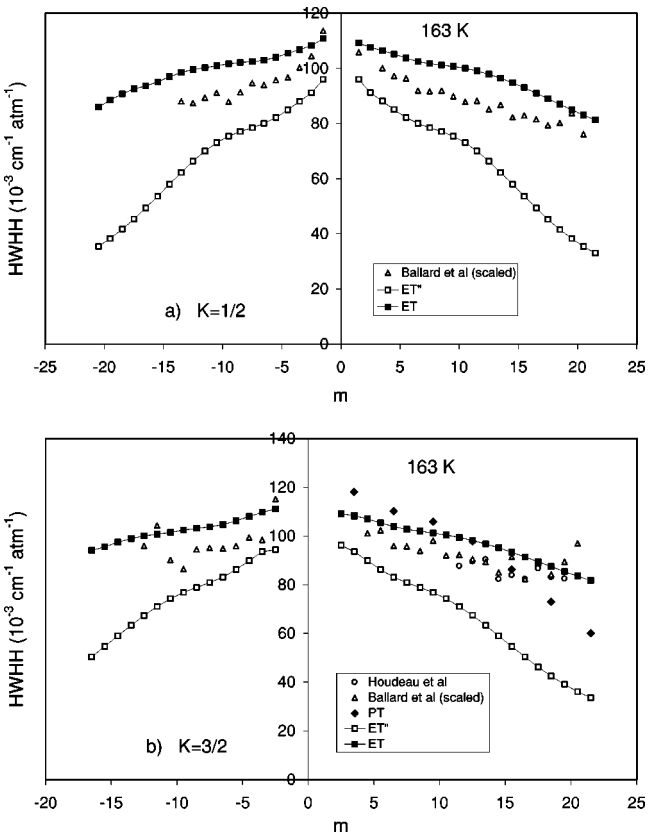

FIG. 6. Line-broadening coefficients as a function of m for the fundamental band of NO perturbed by N_2 at 163 K: (a) $^2\Pi_{1/2}$ sub-band, (b) $^2\Pi_{3/2}$ sub-band.

veals that the condition of smallness of the internal momenta as compared to the total momentum is better assured for $K=3/2$.

IV. CONCLUSION

In this paper the exact trajectory approach was extended to the case of a symmetric top active molecule and applied to the calculation of the IR line-broadening coefficients of nitric monoxide perturbed by nitrogen. An exhaustive theoretical analysis of linewidths was realized for temperatures ranging between 163 and 296 K, which is an interval of crucial importance in the simulation of molecular processes for atmospheric purposes. The calculated values improved the scarce theoretical data available in the literature significantly and provided values for unstudied temperatures. At high temperatures, the exact trajectory model showed an excellent consistency with the experimental data. At low temperatures, it yielded predictions of linewidths more reasonable by far than any of the previously employed trajectory shape models. Therefore, provided a refined intermolecular potential is available, the exact trajectory model is expected to serve as a powerful tool for the reliable computation of linewidths.

The realistic results obtained with the exact trajectory model encourage a similar study of linewidths for the case of NO perturbed by oxygen. Straightforward linewidth measurements for this system had been prevented for a long time

TABLE II. Nitrogen broadened NO $^2\Pi_{1/2}$ sub-band linewidths (10^{-3} cm^{-1}/atm) at 295 K.

J	exper. [10]	PT″	PT	ET″	ET′	ET
0.5	62±7	60.1	68.5	53.3	67.4	67.4
1.5				50.5	66.6	66.7
2.5	72±7	54.8	66.1	49.2	66.4	66.5
3.5	61.1±7			47.8	65.9	66.0
4.5	62.9±7	51.5	63.9	46.2	65.2	65.3
5.5	62.1±6			44.6	64.3	64.4
6.5	63.3±6			43.3	63.5	63.7
7.5	60.8±6			42.3	63.0	63.1
8.5	60.2±6			41.5	62.6	62.7
9.5	65±6	44.0	59.4	40.8	62.3	62.4
10.5	59.3±6	42.6	58.6	40.0	62.0	62.2
11.5	58.6±6			39.1	61.7	61.9
12.5	61.1±6			38.0	61.3	61.5
13.5	61.9±6			36.6	60.8	61.0
14.5	57.5±6			35.0	60.1	60.4
15.5	55.6±6			33.2	59.4	59.7
16.5	57.2±6	29.4	49.4	31.4	58.6	58.9
17.5	57±6			29.5	57.7	58.1
18.5	54.8±6			27.6	56.7	57.2
19.5	55.4±6			25.8	55.7	56.2
20.5	56.5±6	19.3	39.9	24.0	54.6	55.2
21.5	51.4±6			22.4	53.5	54.3
22.5	52±6			20.8	52.4	53.3

TABLE III. Nitrogen-broadened NO $^2\Pi_{3/2}$ sub-band linewidths (10^{-3} cm^{-1}/atm) at 295 K.

J	exper. [10]	PT″	PT	ET″	ET′	ET
1.5				53.9	67.7	67.8
2.5	72±7	59.3	68.4	52.6	67.5	67.6
3.5	68.4±7			50.6	66.9	67.0
4.5	68.2±7	54.7	65.8	48.5	66.1	66.2
5.5	67.3±7			46.6	65.2	65.3
6.5	63±6			44.9	64.3	64.4
7.5	62.3±6			43.5	63.6	63.7
8.5	66.6±6			42.5	63.0	63.2
9.5	63.8±6	45.5	60.3	41.6	62.6	62.8
10.5	62.3±6	43.9	59.4	40.7	62.3	62.5
11.5	64.2±6			39.7	61.9	62.1
12.5	60.7±6			38.4	61.5	61.7
13.5	61.8±6			37.0	60.9	61.2
14.5	60.3±6			35.4	60.3	60.6
15.5	55.4±6			33.6	59.5	59.8
16.5	57.8±6	30.3	50.2	31.8	58.7	59.1
17.5	60.8±6			29.8	57.8	58.2
18.5	55.7±6			28.0	56.8	57.3
19.5	53.2±6			26.1	55.8	56.4
20.5	54.2±6	20	40.7	24.3	54.8	55.4

because of its high reactivity. Only recently have such experimental data become available by Chackerian *et al.* [25] and Allout *et al.* [26]. A few theoretical values presently available for NO-O_2 have been obtained in the framework of the RB approach with the parabolic trajectory model [10] and, despite their roughness, are included in the HITRAN-96 database [11] for air-broadened nitrogen oxide linewidths. The implementation of the exact trajectory model will therefore be particularly valuable for this system and is in progress at our institute.

APPENDIX

Second-order contributions $S_2 \equiv S_{2,i2} + S_{2,f2} + S^{(C)}_{2,f2i2}$ and $S^{(L)}_2$ needed for the computations:

$$ {}_{121}S_2^{D^0D^0} = \frac{\hbar^{-2}}{v^2 r_c^{28}} \left(\sum_{i,j} r_{1i} r_{2j}^2 d_{ij} \right)^2 \left[\sum_{j_i', j_2'} C^{(1)}_{j_i'K} C^{(2)}_{j_2'0} f^{D^0D^0}_{121} + \sum_{j_f', j_2'} C^{(1)}_{j_f'K} C^{(2)}_{j_2'0} f^{D^0D^0}_{121} \right], $$

$$ {}_{121}S_2^{E^0E^0} = \frac{\hbar^{-2}}{v^2 r_c^{16}} \left(\sum_{i,j} r_{1i} r_{2j}^2 e_{ij} \right)^2 \left[\sum_{j_i', j_2'} C^{(1)}_{j_i'K} C^{(2)}_{j_2'0} f^{E^0E^0}_{121} + \sum_{j_f', j_2'} C^{(1)}_{j_f'K} C^{(2)}_{j_2'0} f^{E^0E^0}_{121} \right], $$

$$ {}_{121}S_2^{D^0E^0} = \frac{\hbar^{-2}}{v^2 r_c^{22}} \left(\sum_{i,j} r_{1i} r_{2j}^2 d_{ij} \right) \left(\sum_{i,j} r_{1i} r_{2j}^2 e_{ij} \right) \left[\sum_{j_i', j_2'} C^{(1)}_{j_i'K} C^{(2)}_{j_2'0} f^{D^0E^0}_{121} + \sum_{j_f', j_2'} C^{(1)}_{j_f'K} C^{(2)}_{j_2'0} f^{D^0E^0}_{121} \right], $$

$$ {}_{123}S_2^{\mathrm{el}} = \frac{\hbar^{-2}}{v^2 r_c^{6}} \mu_1^2 Q_2^2 \left[\sum_{j_i', j_2'} C^{(1)}_{j_i'K} C^{(2)}_{j_2'0} f^{\mathrm{el}}_{123} + \sum_{j_f', j_2'} C^{(1)}_{j_f'K} C^{(2)}_{j_2'0} f^{\mathrm{el}}_{123} \right], $$

$$ {}_{123}S_2^{D^0D^0} = \frac{\hbar^{-2}}{v^2 r_c^{28}} \left(\sum_{i,j} r_{1i} r_{2j}^2 d_{ij} \right)^2 \left[\sum_{j_i', j_2'} C^{(1)}_{j_i'K} C^{(2)}_{j_2'0} f^{D^0D^0}_{123} + \sum_{j_f', j_2'} C^{(1)}_{j_f'K} C^{(2)}_{j_2'0} f^{D^0D^0}_{123} \right], $$

$$ {}_{123}S_2^{E^0E^0} = \frac{\hbar^{-2}}{v^2 r_c^{16}} \left(\sum_{i,j} r_{1i} r_{2j}^2 e_{ij} \right)^2 \left[\sum_{j_i', j_2'} C^{(1)}_{j_i'K} C^{(2)}_{j_2'0} f^{E^0E^0}_{123} + \sum_{j_f', j_2'} C^{(1)}_{j_f'K} C^{(2)}_{j_2'0} f^{E^0E^0}_{123} \right], $$

$$ {}_{123}S_2^{D^0E^0} = \frac{\hbar^{-2}}{v^2 r_c^{22}} \left(\sum_{i,j} r_{1i} r_{2j}^2 d_{ij} \right) \left(\sum_{i,j} r_{1i} r_{2j}^2 e_{ij} \right) \left[\sum_{j_i', j_2'} C^{(1)}_{j_i'K} C^{(2)}_{j_2'0} f^{D^0E^0}_{123} + \sum_{j_f', j_2'} C^{(1)}_{j_f'K} C^{(2)}_{j_2'0} f^{D^0E^0}_{123} \right], $$

$$ {}_{123}S_2^{D^0\mathrm{el}} = \frac{\hbar^{-2}}{v^2 r_c^{17}} \left(\sum_{i,j} r_{1i}^2 r_{2j} d_{ij} \right) \mu_1 Q_2 \left[\sum_{j_i', j_2'} C^{(1)}_{j_i'K} C^{(2)}_{j_2'0} f^{D^0\mathrm{el}}_{123} + \sum_{j_f', j_2'} C^{(1)}_{j_f'K} C^{(2)}_{j_2'0} f^{D^0\mathrm{el}}_{123} \right], $$

$$ {}_{123}S_2^{E^0\mathrm{el}} = \frac{\hbar^{-2}}{v^2 r_c^{11}} \left(\sum_{i,j} r_{1i} r_{2j}^2 e_{ij} \right) \mu_1 Q_2 \left[\sum_{j_i', j_2'} C^{(1)}_{j_i'K} C^{(2)}_{j_2'0} f^{E^0\mathrm{el}}_{123} + \sum_{j_f', j_2'} C^{(1)}_{j_f'K} C^{(2)}_{j_2'0} f^{E^0\mathrm{el}}_{123} \right], $$

$$ {}_{224}S_2^{\mathrm{el}} = \frac{\hbar^{-2}}{v^2 r_c^{8}} Q_1^2 Q_2^2 \left[\sum_{j_i', j_2'} C^{(2)}_{j_i'K} C^{(2)}_{j_2'0} f^{\mathrm{el}}_{224} + \sum_{j_f', j_2'} C^{(2)}_{j_f'K} C^{(2)}_{j_2'0} f^{\mathrm{el}}_{224} + D C^{(2)}_{j_2'0} f^{\mathrm{el}}_{224} \right], $$

$$ {}_{224}S_2^{(L)\,\mathrm{el}} = \frac{\hbar^{-2}}{v^2 r_c^{8}} Q_1^2 Q_2^2 D \sum_{j_2' \neq j_2} C^{(2)}_{j_2'0} f^{\mathrm{el}}_{224}, $$

$$ {}_{224}S_2^{D^0D^0} = \frac{\hbar^{-2}}{v^2 r_c^{30}} \left(\sum_{i,j} r_{1i}^2 r_{2j}^2 d_{ij} \right)^2 \left[\sum_{j_i', j_2'} C^{(2)}_{j_i'K} C^{(2)}_{j_2'0} f^{D^0D^0}_{224} + \sum_{j_f', j_2'} C^{(2)}_{j_f'K} C^{(2)}_{j_2'0} f^{D^0D^0}_{224} + D C^{(2)}_{j_2'0} f^{D^0D^0}_{224} \right], $$

TABLE IV. Nitrogen-broadened NO $^2\Pi_{1/2}$ sub-band linewidths (10^{-3} cm^{-1}/atm) at 296 K.

m	exper. [12]	exper. [13]	ET″	ET	m	exper. [12]	exper. [13]	ET″	ET
−1.5	66.8±2	72.2±4.2	53.0	67.8	1.5	68.6±3.4		53.0	65.8
−2.5	58.9±3	66.8±2	50.2	65.9	2.5	66.7±1		50.3	65.1
−3.5	63.8±1.2	64.5±1.7	48.9	65.1	3.5	61.3±1.2	65.1±1.2	49.0	64.9
−4.5	60.4±1	63.7±1	47.6	64.6	4.5	60.4±1.2	63.3±1	47.6	64.4
−5.5	59.6±1.1	62.3±0.7	46.0	63.8	5.5	60.8±1.7	61.6±1	46.0	63.6
−6.5	56.9±0.9	61.9±1.2	44.4	64.0	6.5	58.8±1.5	60.9±1.7	44.4	62.8
−7.5	56.2±2.1	59.8±1.2	43.1	62.4	7.5	58.1±1.1	60.7±1	43.1	62.1
−8.5	55.5±0.6	60.1±1.5	42.2	62.0	8.5	55±1.3	60.2±0.8	42.2	61.5
−9.5	56.2±1.5	60±1.7	41.4	61.6	9.5	52.6±2.1	59.5±0.5	41.4	61.2
−10.5	56.7±1.8	58.6±2.4	40.8	61.4	10.5	51.4±2.8	58.9±0.7	40.8	60.9
−11.5	55.8±1.2	59.6±5	40.1	61.2	11.5	54.9±1.5	58.1±0.8	40.1	60.6
−12.5	55.2±0.6	57.2±2.9	39.2	61.1	12.5	55.5±1	58.1±0.9	39.2	60.3
−13.5	54±0.6	55.3±4.2	38.1	60.9	13.5	49.6±2.5	57.5±0.5	38.1	60.0
−14.5	57.4±2.6		36.8	60.4	14.5	54.8±1	56.8±1	36.8	59.5
−15.5	53.1±1.8		35.2	59.9	15.5	52±1.2	56.6±0.9	35.2	59.0
−16.5	52.4±1.4		33.5	59.4	16.5	54.6±2.9	55.3±1.9	33.5	58.3
−17.5	56.3±1.9		31.6	59.0	17.5	52.8±2	55.5±1.4	31.6	57.6
−18.5	51.3±2		29.8	58.4	18.5	53±1.44	54.4±1.5	29.7	56.8
−19.5	46.3±1		27.9	57.5	19.5	52.7±1.5	52.6±1.6	27.9	55.9
					20.5	52±1.7	54.8±3.9	26.0	55.0
					21.5	50.3±3.0		24.3	54.1

$$ {}_{224}S_2^{(L)D^0D^0} = \frac{\hbar^{-2}}{v^2 r_c^{30}} \left(\sum_{i,j} r_{1i}^2 r_{2j}^2 d_{ij} \right)^2 D \sum_{j_2' \neq j_2} C_{j_2' 0}^{(2)} f_{224}^{D^0 D^0}, $$

$$ {}_{224}S_2^{E^0E^0} = \frac{\hbar^{-2}}{v^2 r_c^{18}} \left(\sum_{i,j} r_{1i}^2 r_{2j}^2 e_{ij} \right)^2 \left[\sum_{j_i', j_2'} C_{j_i' K}^{(2)} C_{j_2' 0}^{(2)} f_{224}^{E^0E^0} + \sum_{j_f', j_2'} C_{j_f' K}^{(2)} C_{j_2' 0}^{(2)} f_{224}^{E^0E^0} + D C_{j_2 0}^{(2)} f_{224}^{E^0E^0} \right], $$

$$ {}_{224}S_2^{(L)E^0E^0} = \frac{\hbar^{-2}}{v^2 r_c^{18}} \left(\sum_{i,j} r_{1i}^2 r_{2j}^2 e_{ij} \right)^2 D \sum_{j_2' \neq j_2} C_{j_2' 0}^{(2)} f_{224}^{E^0E^0}, $$

$$ {}_{224}S_2^{D^0E^0} = \frac{\hbar^{-2}}{v^2 r_c^{24}} \left(\sum_{i,j} r_{1i}^2 r_{2j}^2 d_{ij} \right) \left(\sum_{i,j} r_{1i}^2 r_{2j}^2 e_{ij} \right) \left[\sum_{j_i', j_2'} C_{j_i' K}^{(2)} C_{j_2' 0}^{(2)} f_{224}^{D^0E^0} + \sum_{j_f', j_2'} C_{j_f' K}^{(2)} C_{j_2' 0}^{(2)} f_{224}^{D^0E^0} + D C_{j_2 0}^{(2)} f_{224}^{D^0E^0} \right], $$

$$ {}_{224}S_2^{(L)D^0E^0} = \frac{\hbar^{-2}}{v^2 r_c^{24}} \left(\sum_{i,j} r_{1i}^2 r_{2j}^2 d_{ij} \right) \left(\sum_{i,j} r_{1i}^2 r_{2j}^2 e_{ij} \right) D \sum_{j_2' \neq j_2} C_{j_2' 0}^{(2)} f_{224}^{D^0E^0}, $$

$$ {}_{224}S_2^{D^0\mathrm{el}} = \frac{\hbar^{-2}}{v^2 r_c^{19}} \left(\sum_{i,j} r_{1i}^2 r_{2j}^2 d_{ij} \right) Q_1 Q_2 \left[\sum_{j_i', j_2'} C_{j_i' K}^{(2)} C_{j_2' 0}^{(2)} f_{224}^{D^0\mathrm{el}} + \sum_{j_f', j_2'} C_{j_f' K}^{(2)} C_{j_2' 0}^{(2)} f_{224}^{D^0\mathrm{el}} + D C_{j_2 0}^{(2)} f_{224}^{D^0\mathrm{el}} \right], $$

$$ {}_{224}S_2^{(L)D^0\mathrm{el}} = \frac{\hbar^{-2}}{v^2 r_c^{19}} \left(\sum_{i,j} r_{1i}^2 r_{2j}^2 d_{ij} \right) Q_1 Q_2 D \sum_{j_2' \neq j_2} C_{j_2' 0}^{(2)} f_{224}^{D^0\mathrm{el}}, $$

$$ {}_{224}S_2^{E^0\mathrm{el}} = \frac{\hbar^{-2}}{v^2 r_c^{13}} \left(\sum_{i,j} r_{1i}^2 r_{2j}^2 e_{ij} \right) Q_1 Q_2 \left[\sum_{j_i', j_2'} C_{j_i' K}^{(2)} C_{j_2' 0}^{(2)} f_{224}^{E^0\mathrm{el}} + \sum_{j_f', j_2'} C_{j_f' K}^{(2)} C_{j_2' 0}^{(2)} f_{224}^{E^0\mathrm{el}} + D C_{j_2 0}^{(2)} f_{224}^{E^0\mathrm{el}} \right], $$

TABLE V. Nitrogen-broadened NO $^2\Pi_{3/2}$ sub-band linewidths (10^{-3} cm^{-1}/atm) at 296 K.

m	exper. [12]	exper. [13]	ET″	ET	m	exper. [12]	exper. [13]	ET″	ET
−2.5	67.5±1.5	75.4±4.5	52.2	67.8					
−3.5	66.1±2.4	66.4±2.8	52.2	67.0	3.5	64.6±3.2	67±3.3	52.3	65.9
−4.5	64.3±3.0	67.4±2	50.3	66.1	4.5	64.9±1.8	66.2±1.2	50.3	65.3
−5.5	62±1.6	63.5±1.6	48.3	65.1	5.5	63±0.5	65.8±1.5	48.3	64.5
−6.5	61.2±0.6	64.3±1.5	46.3	64.1	6.5	62.3±0.7	64.3±1.2	46.3	63.6
−7.5	60.1±2.3	63.8±1.7	44.7	63.3	7.5	61.8±1.3	63.8±1.1	44.7	62.8
−8.5	59.2±1.8	61.5±3.3	43.4	62.7	8.5	59.1±1.5	63.3±0.9	43.4	62.1
−9.5	60.6±0.3	63±3.3	42.4	62.2	9.5	57.8±0.9	62±1.1	42.4	61.6
−10.5	57.6±0.9	62.3±4	41.6	61.8	10.5	57±2.4	60.6±1	41.6	61.2
−11.5	57.9±3.4	58.5±5.4	40.7	61.6	11.5	59.3±2.5	60.4±1	40.7	60.9
−12.5	58.7±3.8	58.5±4.5	39.8	61.4	12.5	56±0.2	61.4±0.8	39.7	60.6
−13.5	56±1.0		38.6	61.1	13.5	57.4±1.8	59.2±1.3	38.6	60.2
−14.5	55.5±0.8		37.2	60.6	14.5	58±1.2	57.7±2	37.2	59.7
−15.5	60.9±2.5		35.6	60.1	15.5	54.8±1.2	58.8±1.8	35.6	59.1
−16.5	56.9±0.4		33.8	59.6	16.5	53.8±2.1	57.2±2.9	33.8	58.4
−17.5					17.5	54.8±0.7	59.2±2.6	32.0	57.7
−18.5	41.8±2.9		30.1	58.5	18.5	54.8±1.9	55.1±3.5	30.1	56.9
−19.5					19.5	47±2.7	58.2±3.8	28.2	56.1
−20.5	46.8±7.4		26.4	56.7	20.5	57.8±1.6	58.4±8.8	26.4	55.2
−21.5	51±11.0		24.6	56.1	21.5	56.7±2.4		24.6	54.3

$$ {}_{224}S_2^{(L)E^0\mathrm{el}} = \frac{\hbar^{-2}}{v^2 r_c^{13}} \left(\sum_{i,j} r_{1i}^2 r_{2j}^2 e_{ij} \right) Q_1 Q_2 D \sum_{j_2' \neq j_2} C_{j_2'0}^{(2)} f_{224}^{E^0\mathrm{el}}, $$

$$ {}_{224}S_2^{D^1D^1} = \frac{\hbar^{-2}}{v^2 r_c^{34}} \left(\sum_{i,j} r_{1i}^2 r_{2j}^2 (r_{1i}^2 + r_{2j}^2) d_{ij} \right)^2 \left[\sum_{j_i', j_2'} C_{j_i'K}^{(2)} C_{j_2'0}^{(2)} f_{224}^{D^1D^1} + \sum_{j_f', j_2'} C_{j_f'K}^{(2)} C_{j_2'0}^{(2)} f_{224}^{D^1D^1} + D C_{j_20}^{(2)} f_{224}^{D^1D^1} \right], $$

$$ {}_{224}S_2^{(L)D^1D^1} = \frac{\hbar^{-2}}{v^2 r_c^{34}} \left(\sum_{i,j} r_{1i}^2 r_{2j}^2 (r_{1i}^2 + r_{2j}^2) d_{ij} \right)^2 D \sum_{j_2' \neq j_2} C_{j_2'0}^{(2)} f_{224}^{D^1D^1}, $$

$$ {}_{224}S_2^{D^0D^1} = \frac{\hbar^{-2}}{v^2 r_c^{32}} \left(\sum_{i,j} r_{1i}^2 r_{2j}^2 d_{ij} \right) \left(\sum_{i,j} r_{1i}^2 r_{2j}^2 (r_{1i}^2 + r_{2j}^2) d_{ij} \right) \left[\sum_{j_i', j_2'} C_{j_i'K}^{(2)} C_{j_2'0}^{(2)} f_{224}^{D^0D^1} + \sum_{j_f', j_2'} C_{j_f'K}^{(2)} C_{j_2'0}^{(2)} f_{224}^{D^0D^1} + D C_{j_20}^{(2)} f_{224}^{D^0D^1} \right], $$

$$ {}_{224}S_2^{(L)D^0D^1} = \frac{\hbar^{-2}}{v^2 r_c^{32}} \left(\sum_{i,j} r_{1i}^2 r_{2j}^2 d_{ij} \right) \left(\sum_{i,j} r_{1i}^2 r_{2j}^2 (r_{1i}^2 + r_{2j}^2) d_{ij} \right) D \sum_{j_2' \neq j_2} C_{j_2'0}^{(2)} f_{224}^{D^0D^1}, $$

$$ {}_{224}S_2^{E^0D^1} = \frac{\hbar^{-2}}{v^2 r_c^{26}} \left(\sum_{i,j} r_{1i}^2 r_{2j}^2 e_{ij} \right) \left(\sum_{i,j} r_{1i}^2 r_{2j}^2 (r_{1i}^2 + r_{2j}^2) d_{ij} \right) \left[\sum_{j_i', j_2'} C_{j_i'K}^{(2)} C_{j_2'0}^{(2)} f_{224}^{E^0D^1} + \sum_{j_f', j_2'} C_{j_f'K}^{(2)} C_{j_2'0}^{(2)} f_{224}^{E^0D^1} + D C_{j_20}^{(2)} f_{224}^{E^0D^1} \right], $$

$$ {}_{224}S_2^{(L)E^0D^1} = \frac{\hbar^{-2}}{v^2 r_c^{26}} \left(\sum_{i,j} r_{1i}^2 r_{2j}^2 e_{ij} \right) \left(\sum_{i,j} r_{1i}^2 r_{2j}^2 (r_{1i}^2 + r_{2j}^2) d_{ij} \right) D \sum_{j_2' \neq j_2} C_{j_2'0}^{(2)} f_{224}^{E^0D^1}, $$

$$ {}_{224}S_2^{\mathrm{el}\,D^1} = \frac{\hbar^{-2}}{v^2 r_c^{21}} \left(\sum_{i,j} r_{1i}^2 r_{2j}^2 (r_{1i}^2 + r_{2j}^2) d_{ij} \right) Q_1 Q_2 \left[\sum_{j_i', j_2'} C_{j_i'K}^{(2)} C_{j_2'0}^{(2)} f_{224}^{\mathrm{el}\,D^1} + \sum_{j_f', j_2'} C_{j_f'K}^{(2)} C_{j_2'0}^{(2)} f_{224}^{\mathrm{el}\,D^1} + D C_{j_20}^{(2)} f_{224}^{\mathrm{el}\,D^1} \right], $$

$$_{224}S_2^{(L)\mathrm{el}D^1}=\frac{\hbar^{-2}}{v^2r_c^{21}}\left(\sum_{i,j}r_{1i}^2r_{2j}^2(r_{1i}^2+r_{2j}^2)d_{ij}\right)Q_1Q_2D\sum_{j_2'\neq j_2}C_{j_2'0}^{(2)}f_{224}^{\mathrm{el}\,D^1}.$$

In the above formulas the following notations are introduced: $C_{J'K}^{(n)}\equiv(C_{JKn0}^{J'K})^2$ and $D=(-1)^{j_i+j_f}2[(2j_i+1)(2j_f+1)C_{j_iK}^{(l_1)}C_{j_fK}^{(l_1)}]^{1/2}W(j_ij_fj_ij_f;\nu l_1)$, where $W(j_ij_fj_ij_f;\nu l_1)$ is the Racah coefficient, and ν is the order of the coupling tensor between the moleculear system and the external field; for the IR absorption case considered here, $\nu=1$. The resonance parameter k_c is defined by $k_c=\omega r_c/v$.

Resonance functions:

$$f_{121}^{D^0D^0}=\frac{1517824}{75}\sum_{m\ \mathrm{odd}}\mathcal{M}(1;m)\mathcal{I}^2(14),$$

$$f_{121}^{E^0E^0}=\frac{1024}{3}\sum_{m\ \mathrm{odd}}\mathcal{M}(1;m)\mathcal{I}^2(8),$$

$$f_{121}^{D^0E^0}=-\frac{78848}{15}\sum_{m\ \mathrm{odd}}\mathcal{M}(1;m)\mathcal{I}(14)\mathcal{I}(8),$$

$$f_{123}^{\mathrm{el}}=2\sum_{m\ \mathrm{odd}}\mathcal{M}(3;m)\mathcal{I}^2(3),$$

$$f_{123}^{D^0D^0}=\frac{1605632}{25}\sum_{m\ \mathrm{odd}}\mathcal{M}(3;m)\mathcal{I}^2(14),$$

$$f_{123}^{E^0E^0}=2048\sum_{m\ \mathrm{odd}}\mathcal{M}(3;m)\mathcal{I}^2(8),$$

$$f_{123}^{D^0E^0}=-\frac{114688}{5}\sum_{m\ \mathrm{odd}}\mathcal{M}(3;m)\mathcal{I}(14)\mathcal{I}(8),$$

$$f_{123}^{D^0\mathrm{el}}=\frac{3584}{5}\sum_{m\ \mathrm{odd}}\mathcal{M}(3;m)\mathcal{I}(14)\mathcal{I}(3),$$

$$f_{123}^{E^0\mathrm{el}}=-128\sum_{m\ \mathrm{odd}}\mathcal{M}(3;m)\mathcal{I}(8)\mathcal{I}(3),$$

$$f_{224}^{\mathrm{el}}=\frac{28}{5}\sum_{m\ \mathrm{even}}\mathcal{M}(4;m)\mathcal{I}^2(4),$$

$$f_{224}^{D^0D^0}=\frac{1040449536}{875}\sum_{m\ \mathrm{even}}\mathcal{M}(4;m)\mathcal{I}^2(15),$$

$$f_{224}^{E^0E^0}=\frac{589824}{35}\sum_{m\ \mathrm{even}}\mathcal{M}(4;m)\mathcal{I}^2(9),$$

$$f_{224}^{D^0E^0}=-\frac{49545216}{175}\sum_{m\ \mathrm{even}}\mathcal{M}(4;m)\mathcal{I}(15)\mathcal{I}(9),$$

$$f_{224}^{D^0\mathrm{el}}=\frac{129024}{25}\sum_{m\ \mathrm{even}}\mathcal{M}(4;m)\mathcal{I}(15)\mathcal{I}(4),$$

$$f_{224}^{E^0\mathrm{el}}=-\frac{3072}{5}\sum_{m\ \mathrm{even}}\mathcal{M}(4;m)\mathcal{I}(9)\mathcal{I}(4),$$

$$f_{224}^{D^1D^1}=\frac{10277093376}{35}\sum_{m\ \mathrm{even}}\mathcal{M}(4;m)\mathcal{I}^2(17),$$

$$f_{224}^{D^0D^1}=\frac{6539968512}{175}\sum_{m\ \mathrm{even}}\mathcal{M}(4;m)\mathcal{I}(15)\mathcal{I}(17),$$

$$f_{224}^{E^0D^1}=-\frac{155713536}{35}\sum_{m\ \mathrm{even}}\mathcal{M}(4;m)\mathcal{I}(9)\mathcal{I}(17),$$

$$f_{224}^{\mathrm{el}\,D^1}=\frac{405504}{5}\sum_{m\ \mathrm{even}}\mathcal{M}(4;m)\mathcal{I}(4)\mathcal{I}(17),$$

where

$$\mathcal{M}(l;m)\equiv\frac{(l+m)!(l-m)!}{2^{2l}[(l-m)/2]!^2[(l+m)/2]!^2}$$

and

$$\mathcal{I}(n)\equiv\int_1^\infty dy\,\frac{\cos[A_0(y)k_c+m\{1-V_{\mathrm{iso}}^*(r_c)\}^{1/2}A_2(y)]}{y^n\{y^2-1+V_{\mathrm{iso}}^*(r_c)-y^2V_{\mathrm{iso}}^*(yr_c)\}^{1/2}}.$$

[1] P. W. Anderson, Phys. Rev. **76**, 647 (1949).

[2] C. J. Tsao and B. Curnutte, J. Quant. Spectrosc. Radiat. Transf. **2**, 41 (1962).

[3] D. Robert and J. Bonamy, J. Phys. (Paris) **40**, 923 (1979).

[4] R. Kubo, *Fluctuation. Relaxation and Resonance in Magnetic Systems*, edited by ter Haar (Olivier and Boyd, London, 1962).

[5] A. D. Bykov, N. N. Lavrent'eva, and L. N. Sinitsa, Atmos. Oceanic Opt. **5**, 587 (1992).

[6] A. D. Bykov, N. N. Lavrent'eva, and L. N. Sinitsa, Atmos. Oceanic Opt. **5**, 728 (1992).

[7] L. D. Landau and E. M. Lifshits, *Mechanics*, Vol. 1 of *Course of Theoretical Physics*, 3rd ed. (Pergamon, Oxford, 1976).

[8] J. Buldyreva, J. Bonamy, and D. Robert, J. Quant. Spectrosc. Radiat. Transf. **62**, 321 (1999).

[9] J. Bonamy, A. Khayar, and D. Robert, Chem. Phys. Lett. **83**, 539 (1981).
[10] J. P. Houdeau, C. Boulet, J. Bonamy, A. Khayar, and G. Guelachvili, J. Chem. Phys. **79**, 1634 (1983).
[11] A. Goldman *et al.*, J. Quant. Spectrosc. Radiat. Transf. **60**, 825 (1998).
[12] M. N. Spencer, C. Chackerian, Jr., L. P. Giver, and L. R. Brown, J. Mol. Spectrosc. **181**, 307 (1997).
[13] J. Ballard, W. B. Johnston, B. J. Kerridge, and J. J. Remedios, J. Mol. Spectrosc. **127**, 70 (1988).
[14] R. P. Leavitt, J. Chem. Phys. **72**, 3472 (1980).
[15] L. Hochard-Demolliere, C. Alamichel, and Ph. Arcas, J. Phys. (Paris) **28**, 421 (1967).
[16] M. Oobatake and T. Ooi, Prog. Theor. Phys. **48**, 2132 (1972).
[17] R. P. Leavitt, J. Chem. Phys. **73**, 5432 (1980).
[18] D. A. Varshalovich, A. N. Moskalev, and V. K. Khersonskii, *Quantum Theory of Angular Momentum* (World Scientific, Singapore, 1988).
[19] H. Yasuda and T. Yamamoto, Prog. Theor. Phys. **45**, 1458 (1971).
[20] A. Henry, F. Severin, and L. Henry, J. Mol. Spectrosc. **75**, 495 (1979).
[21] N. Rohrbeck, R. Winter, W. Hermann, J. Wildt, and W. Urban, Mol. Phys. **39**, 673 (1980).
[22] J.-P. Bouanich and G. Blanquet, J. Quant. Spectrosc. Radiat. Transf. **40**, 205 (1989).
[23] J. M. Hartmann, J. Taine, J. Bonamy, B. Labani, and D. Robert, J. Chem. Phys. **86**, 144 (1987).
[24] J. O. Hirschfelder, C. F. Curtiss, and R. B. Burd, *Molecular Theory of Gases and Liquids* (Wiley, New York, 1967).
[25] C. Chackerian, Jr., R. S. Freedman, L. P. Giver, and L. R. Brown, J. Mol. Spectrosc. **192**, 215 (1998).
[26] M.-Y. Allout, V. Dana, J.-Y. Mandin, P. von der Hayden, D. Décatoire, and J.-J. Plateuax, J. Quant. Spectrosc. Radiat. Tranf. **61**, 759 (1999).